Hindawi
Advances in Civil Engineering
Volume 2018, Article ID 8195396, 6 pages
https://doi.org/10.1155/2018/8195396

Research Article

Effects of Spatially Varying Seismic Ground Motions and Incident Angles on Behavior of Long Tunnels

Yundong Zhou, Yongxin Wu, Ziheng Shangguan, and Zhanbin Wang

Key Laboratory of Ministry of Education for Geomechanics and Embankment Engineering, Hohai University, Nanjing 210098, China

Correspondence should be addressed to Yongxin Wu; yxwuhhu@163.com

Received 14 March 2018; Accepted 7 May 2018; Published 11 June 2018

Academic Editor: Yongfeng Deng

Seismic behavior of long circle tunnels is significantly influenced by the nature of input motion. This study, based on the 3D finite-element method (FEM), evaluates the effects of spatially varying seismic ground motions and uniform input seismic ground motions and their incident angles on the diameter strain rate and tensive/compressive principal stresses under different strata. It is found that (1) the spatially varying seismic ground motions induced larger diameter strain rate (radially deformation) than the uniform input seismic motion, (2) the spatially varying seismic ground motions had an asymmetric effect on the radial strain rate distributions, and (3) the rising incident angles changed the pure shear stress state into a complex stress state for tunnels under specified input motion.

1. Introduction

Tunnels, as an integral part of the infrastructure of modern society, would suffer damages when subjected to dynamic loadings during earthquake activity, for example, in Kobe earthquake (1995) [1], Chi-Chi earthquake (1999) [2], Duzce earthquake (1999) [3], Mid-Niigata Prefecture earthquake (2004) [4], Wenchuan earthquake (2008) [5], and Tohoku earthquake (2011) [6]. Nevertheless, the number of large tunnels and underground structures had grown significantly in recent decades. Therefore, seismic evaluation of tunnels in seismically active areas is critical during engineering design.

Seismic behavior of tunnels has been widely studied by many researchers [7–11], and these researches have concentrated mostly on 2D analysis. For the analysis of axial and bending deformations of tunnels, it is most appropriate to utilize 3D models.

However, for the 3D analysis of seismic behavior of tunnel, soil-tunnel analyses in the past were typically limited to relatively small regions, which made it difficult to fully consider the complex spatial features involved in such large structures [12]. Tunnels often had significant length and could be built on different strata foundations, which made the seismic analysis of tunnels a complex problem and was usually evaluated under idealized conditions by using numerical methods, such as the finite-element method (FEM).

For the seismic analysis of complex stress distribution and deformation of long-distance tunnels, it is often more reliable to adopt three-dimensional (3D) methods. With the rapid development of science and technology, it is now possible to use high-performance computers to conduct large-scale 3D FEM seismic analysis for tunnels. There are three kinds of deformation, such as axial compression/extension, longitudinal bending, and ovalling/racking, occurring in tunnels during earthquake [10]. Particularly, the cross-sectional distortion of the tunnel can be related to seismic waves propagating along the tunnel.

Yu et al. [13, 14] presented a multiscale 3D FEM analysis of long tunnels under seismic loads where the mechanical characteristics of the tunnel segments and joints under artificial or recorded earthquake loads were evaluated in detail. The model in this paper would take into account not only the motion distribution with time but also the spatial variability (incoherency effect), the wave-passage effect, and the site-response effect.

This paper, based on an earlier report by the authors [15], attempts to develop a new model for seismic analysis of long tunnels with multisupport excitations, which properly accounts for the spatial variability. The main focus of this paper

is to assess the influence of multisupport input earthquake waves and uniform input earthquake waves as well as their incident angles on the diameter strain rate and tensive/compressive principal stresses under different strata. A full-scale 3D finite-element model is built comprising geological data, tunnel geometry, and so on to farthest simulate actual situation.

2. Simulation of Seismic Ground Motions

2.1. Simulation of Uniform Seismic Ground Motion. Consider a zero mean Gaussian stationary seismic ground motion with a target autospectral density $S(\omega)$. The seismic ground motions can be generated through the following expression:

$$x(t) = 2\sum_{l=1}^{N}\sqrt{S(\omega_l)\Delta\omega}\cos(\omega_l t + \varphi_l), \tag{1}$$

where N is the number of frequency intervals, $\Delta\omega = \omega_u/N$ is frequency increment with ω_u as the cutoff frequency, $\omega_l = l\Delta\omega$, and the φ_l's are statistically independent random phase angles uniformly distributed between $(0, 2\pi]$. Equation (1) is valid if there is an upper cutoff frequency ω_u above which the contribution of the power spectral density (PSD) to the simulations is negligible for practical purposes.

2.2. Simulation of Spatially Varying Seismic Ground Motions. The variations in ground motion are caused by the following four sources: (1) the "incoherence effect," (2) the "wave-passage effect," (3) the "site-response effect," and (4) the "attenuation effect." The spectral representation method is one of the most widely used methods in simulating the spatially varying seismic ground motions.

In practical application, spatially correlated ground motions can be considered as a one-dimensional, n-variety (1D-nV) stochastic vector process $X(t)$ with components $x_j(t) \cdot (j = 1, 2, \ldots, n)$. Based on the spectral representation method, the jth component of the ground motions can be generated by [13]

$$\begin{aligned} x_j(t) &= 2\sum_{k=1}^{n}\sum_{l=1}^{N}\left|H_{jk}(\omega_l)\right|\sqrt{\Delta\omega}\cos\left[\omega_l t - \phi_{jk}(\omega_l) + \varphi_{kl}\right], \\ \omega_l &= l\Delta\omega \quad (l = 0, 1, K, \ldots, N-1), \\ \Delta\omega &= \frac{\omega_u}{N}, \end{aligned} \tag{2}$$

where ω_u is the upper cutoff frequency beyond which elements of the power spectral can be assumed to be zero for either mathematical or physical reasons and φ_{jk} are independent random phase angles uniformly distributed over (0, 2π]. $|H_{jk}(\omega)|$ and $\phi_{jk}(\omega)$ are the modulus and phase parts of $H_{jk}(\omega)$, respectively, which can be obtained by the root decomposition of power spectral density matrix as follows:

$$\mathbf{S}(\omega) = \mathbf{H}(\omega)\mathbf{H}^T(\omega), \tag{3}$$

where the superscript T denotes conjugate transpose.

The power spectral density matrix is given as

$$\mathbf{S}(\omega) = \begin{bmatrix} S_{11}(\omega) & S_{12}(\omega) & \cdots & S_{1m}(\omega) \\ S_{21}(\omega) & S_{22}(\omega) & \cdots & S_{2m}(\omega) \\ \vdots & \vdots & \ddots & \vdots \\ S_{m1}(\omega) & S_{m2}(\omega) & \cdots & S_{mm}(\omega) \end{bmatrix}, \tag{4}$$

where $S_{jj}(\omega)$ is the autopower spectral density function and $S_{jk}(\omega, t)$ is the cross-power spectral density function, which can be expressed as

$$S_{jk}(\omega, t) = \left|\gamma_{jk}(\omega)\right|\sqrt{S_{jj}(\omega)S_{kk}(\omega)}\, e^{i\theta_{jk}(\omega)}, \tag{5}$$

where $|\gamma_{jk}(\omega)|$ is the lagged coherence function representing "incoherence" effect and $\theta_{jk}(\omega)$ is composed of wave passage.

However, the ground motions simulated by the above method are stationary, while the actual seismic records are nonstationary. Therefore, to obtain nonstationary seismic ground motion, the way of multiplying an envelope function is applied. The envelope function is as follows:

$$f(t) = \begin{cases} (t/t_1)^2, & t < t_1 \\ 1, & t_1 \le t < t_2 \\ e^{-c(t-t_2)}, & t \ge t_2 \end{cases}, \tag{6}$$

where t_1, t_2, and c are three parameters describing the shape of the envelope function. In this study, they are set to be $t_1 = 6$, $t_2 = 10$, and $c = 0.5$, respectively.

3. FE Model

The tunnel model adopted in this paper was built with circular appearance, whose outside diameter is 10 m, inside diameter is 9 m, and length is 1000 m. It had a buried depth of 30 m from the tunnel center to soil surface. The simulation setup is shown in Figure 1. It consists of a $1000 \times 300 \times 100$ m box with the 1000 m length circular tunnel. The space coordinates were built by taking the length direction as the Z-axis, the width direction as the X-axis, and the height direction as the Y-direction. The soil profile was modeled as four layers of Mohr–Coulomb materials and tunnel as the elastic material. All the property parameters used can be found in Tables 1 and 2. An infinite domain by using the artificial boundary was adopted [12], where both borders of the tunnel were fixed in the Z-direction.

In this work, the constitutive model of the tunnel is an elastic model, which is given as follows:

$$\boldsymbol{\sigma} = \lambda I_1 \boldsymbol{\delta} + 2G\boldsymbol{\varepsilon}, \tag{7}$$

in which $\boldsymbol{\sigma}$ is the stress tensor, $\boldsymbol{\varepsilon}$ is the strain tensor, I_1 is the first strain invariant, λ is the Lame constant, and G is the shear modulus.

The Mohr–Coulomb yield criterion for soil is expressed as follows:

$$\begin{aligned} \frac{m+1}{2}\max\Big(&\left|\sigma_1 - \sigma_2\right| + K(\sigma_1 + \sigma_2), \left|\sigma_1 - \sigma_3\right| \\ &+K(\sigma_1 + \sigma_3), \left|\sigma_2 - \sigma_3\right| + K(\sigma_2 + \sigma_3)\Big) = S_{yc}, \end{aligned} \tag{8}$$

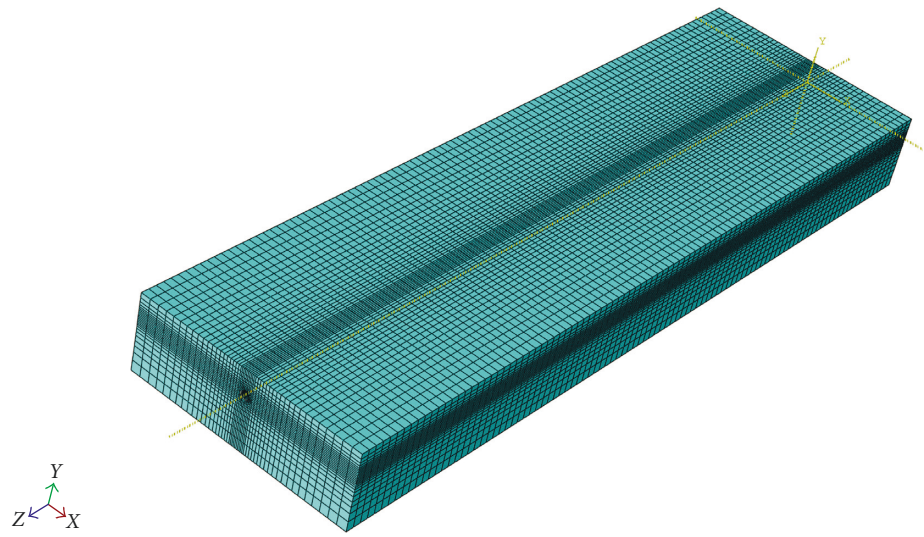

Figure 1: Finite-element mesh model adopted in the 3D FE analyses for soil with long tunnels.

Table 1: Properties of different soil layers.

Layer number	Young's modulus (MPa)	Poisson's ratio	Density (kg/m^3)	Cohesion (kPa)	Internal friction angle (°)	Thickness (m)
1	3.029	0.45	1760	10.8	14.2	20.6
2	6.135	0.36	1810	17.7	18.9	23.9
3	6.319	0.47	1870	22	22.9	24.2
4	6.251	0.36	1950	24.9	18.2	31.5

Table 2: Properties of the tunnel.

Elastic modulus (kg/m^3)	Poisson's ratio	Unit weight (kN/m^3)
3.6*e*7	0.2	25.7

where

$$m = \frac{S_{yc}}{S_{yt}}, \qquad K = \frac{m-1}{m+1}, \tag{9}$$

and the parameters S_{yc} and S_{yt} are the yield stresses of the material in uniaxial compression and tension, respectively.

On the interface, the deformation of the tunnel and soil is in concert and harmony.

4. Computation and Analysis

In computation, a regular 3D finite-element model was built based on geotechnical data, tunnel geometry, and so on. The traveling waves velocity motivated from bedrock surface was 500 m/s in the 3D spatially varying seismic ground motion field. The schematic diagram of different incident angles used is shown in Figure 2. The simulated spatially varying ground motions are plotted in Figure 3.

4.1. Effect on Radial Deformations. The diameter strain rate Δd is defined as

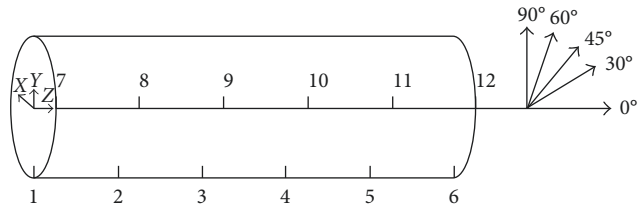

Figure 2: The schematic diagram at different incident angles.

$$\Delta d = \frac{d' - d}{d}, \tag{10}$$

where d and d' are the tunnel diameters before and after deformation.

The positive rate value denotes that the tunnel cross section undergoes tensile deformation in radial direction, and the negative value corresponds to compressive deformation. In this section, d_{max} is defined as the maximum of Δd in the earthquake time process. d_{max} in the vertical direction is calculated from displacement time processes at the vertex and nadir of tunnel in the Y-axis direction while the one in the lateral direction is obtained from processes at the right and left sides of the tunnel in the X-axis direction. It was found from the simulation that lateral Δd and vertical Δd were equal and opposite in the direction at any arbitrary time, videlicet, the primary deformation of tunnel under seismic waves was ovalling. In addition, the partial feature results under uniform and spatially varying seismic ground motions, that is, the lateral d_{max} at $Z = 100$ m, 300 m, 500 m, 700 m, and

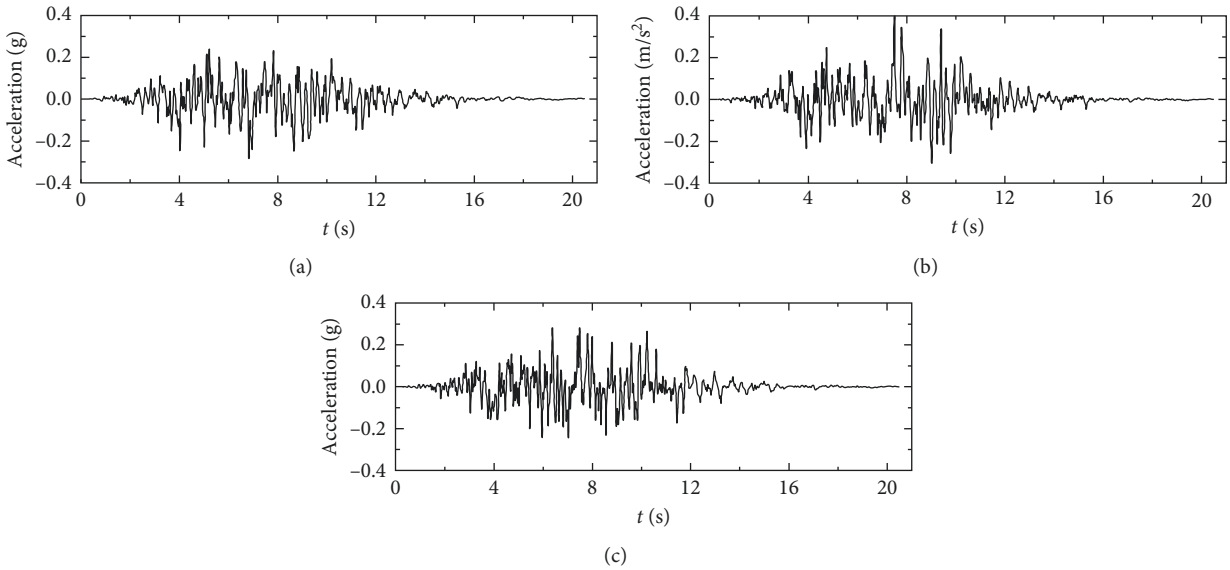

Figure 3: The simulated spatially varying seismic ground motions: (a) $x = 0$ m, (b) $x = 500$ m, and (c) $x = 1000$ m.

Table 3: Lateral maximum diameter strain rate of tunnel under uniform seismic motion.

Incident angle	$Z = 100$ m	$Z = 300$ m	$Z = 500$ m	$Z = 700$ m	$Z = 900$ m
0°	−0.036%	−0.004%	0	−0.004%	−0.036%
30°	0.087%	0.113%	0.118%	0.113%	0.087%
45°	0.130%	0.158%	0.165%	0.158%	0.130%
60°	0.171%	0.196%	0.204%	0.196%	0.171%
90°	0.214%	0.226%	0.236%	0.226%	0.214%

Table 4: Lateral maximum diameter strain rate of tunnel under multisupport seismic motion.

Incident angle	$Z = 100$ m	$Z = 300$ m	$Z = 500$ m	$Z = 700$ m	$Z = 900$ m
0°	0.022%	−0.045%	0.033%	0.035%	0.039%
30°	0.075%	−0.125%	−0.169%	−0.169%	−0.098%
45°	0.111%	−0.163%	−0.225%	−0.225%	−0.123%
60°	0.141%	−0.193%	−0.269%	−0.269%	−0.143%
90°	0.170%	−0.208%	−0.293	−0.293%	−0.155%

900 m with incident angles of 0°, 30°, 45°, 60°, and 90° can be found in Tables 3 and 4.

It could be observed that the lateral $d_{\max}$ increases with increasing incident angles for both seismic input forms, but the maximum positions differ from each other. For uniform seismic input simulations, the lateral $d_{\max}$ position is at the middle point ($Z = 500$ m) of the tunnel and the diameter strain rates are symmetrically distributed on the left and right sides of the tunnel. This can be attributed to the balanced boundary conditions and uniform seismic waves. For spatially varying seismic ground motions, the lateral $d_{\max}$ is located between $Z = 700$ m and $Z = 900$ m and exhibits asymmetric features due to the nonuniform waves. The table also implies that the lateral $d_{\max}$ for the whole tunnel under spatially varying seismic ground motions is greater than that under uniform input ground motions.

4.2. Effect on Stress Distributions. The maximum principal shear ($\sigma_{t\max}$) and compressive ($\sigma_{c\max}$) stresses are commonly used to analyze the effect of seismic input ground motions on tunnels. The peak stresses under different incident angles are illustrated in Table 5.

It is indicated that the maximum tensile stress is identical to the maximum compressive stress while the incident angle is 0° for uniform seismic input tunnels. This is owing to the tunnel and soil profile placed in pure shear stress state. When incident angles are equal to 30°, 45°, 60°, and 90°, the values of maximum tensile and compressive stresses are different because of the complex shear and normal stress states induced by seismic load. It can be thus concluded that the earthquake acceleration in the vertical direction changes not only the maximum stress but also the stress characteristics. In addition, the spatially varying seismic ground motion is another factor influencing the stress state according to the different values between the maximum tensile stress and maximum compressive stress at an incident angle of 0° under spatially varying seismic ground motions. Meanwhile, the value of maximum tensile/compressive stresses decreases with the increasing incident angles. The maximum tensile stress nephogram at an incident angle of 0° for both uniform and spatially varying seismic ground motions is, respectively, shown in Figures 4 and 5.

Table 5: Maximum stresses of tunnel body at different incident angles.

Motion form	Principal stress	0°	30°	45°	60°	90°
Uniform	$\sigma_{t\max}$	11.60	10.85	9.24	7.18	7.45
	$\sigma_{c\max}$	−11.60	−10.58	−10.02	−8.99	−6.81
Multisupport	$\sigma_{t\max}$	17.74	13.92	11.29	8.94	6.66
	$\sigma_{c\max}$	−18.84	−15.68	−13.37	−11.16	−8.49

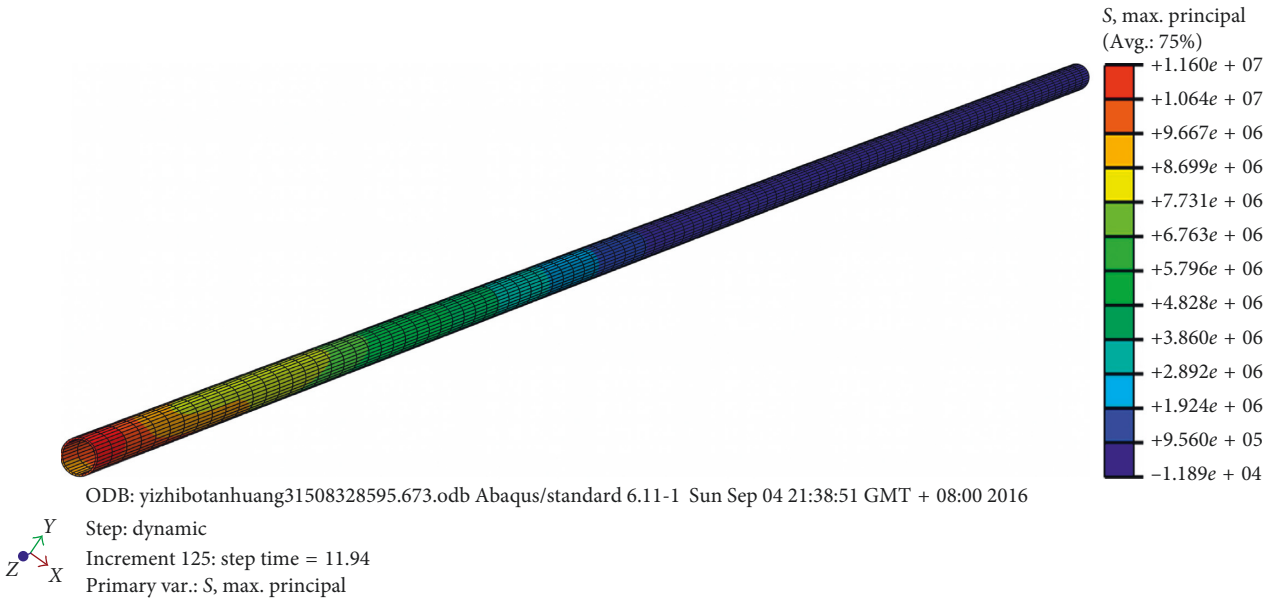

Figure 4: The maximum tensile stress nephogram at an incident angle of 0° under uniform seismic input motion.

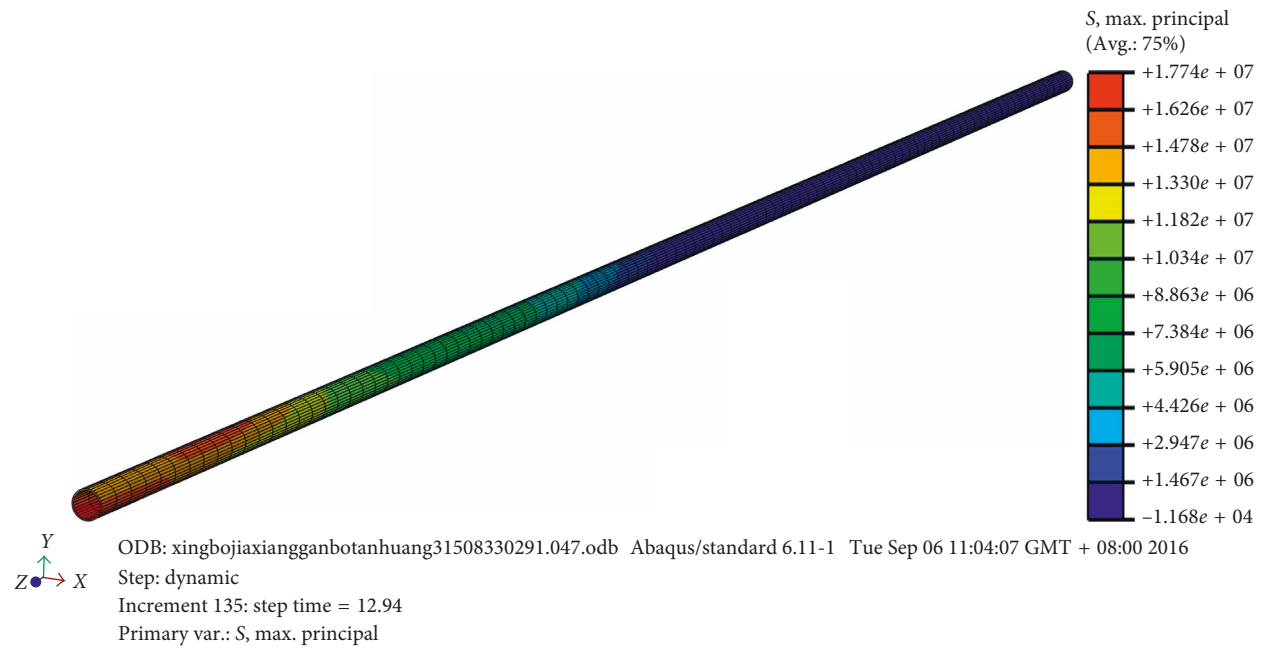

Figure 5: The maximum tensile stress nephogram at an incident angle of 0° under multisupport seismic input motion.

The red upper portion of the tunnel end ($Z = 1000$ m) in Figure 4 is the maximum tensile stress, responding to the red lower portion near the tunnel end. It is suggested that the spatially varying seismic ground motion affects the stress distribution.

5. Conclusions

Numerical simulation was an effective method for studying the tunnel responses under seismic event. In this paper, a novel large-scale analytical method was established for estimating the seismic response of long tunnels within soil foundations. Based on the 3D FEM platform, this method could offer a reliable way for investigating the nonlinear seismic behavior of long tunnels. Main findings are summarized as follows:

(1) The spatially varying seismic ground motions induced larger diameter strain rates (radial deformation) than the uniform input seismic motion. The maximum radial strain rate increased with the increasing incident angles for both seismic input forms.

(2) For uniform seismic input simulations, the maximum radial strain rate occurred at the middle point of the tunnel and the radial strain rates were symmetrically distributed on the left and right sides of the tunnel. Moreover, the spatially varying seismic

ground motions had an asymmetric effect on the radial strain rate distributions.

(3) The rising incident angles changed the pure shear stress state into a complex stress state for tunnels under specified input motion. The spatially varying seismic ground motions also influenced the stress state relative to the uniform seismic input. Meanwhile, the values of maximum tensile/compressive stresses decreased with the increasing incident angles.

Data Availability

All the data supporting the conclusions of this study are presented in the tables of the article. The code and details of the FEM for the analysis are available upon request from the corresponding author.

Conflicts of Interest

The authors declare that they have no conflicts of interest.

Acknowledgments

The supports by the National Natural Science Foundation of China (Grant no. 41630638), the National Key Basic Research Program of China (Grant no. 2015CB057901), and the Fundamental Research Funds for the Central Universities (Grant no. 2018B13914) are greatly acknowledged.

References

[1] H. Iida, T. Hiroto, N. Yoshida et al., "Damage to Daikai subway station," *Soils and Foundations*, vol. 36, pp. 283–300, 1996.

[2] W. L. Wang, T. T. Wang, J. J. Su et al., "Assessment of damage in mountain tunnels due to the Taiwan Chi-Chi earthquake," *Tunnelling and Underground Space Technology*, vol. 16, no. 3, pp. 133–150, 2001.

[3] C. Menkiti, R. Mair, and R. Miles, "Highway tunnel performance during the 1999 Duzce earthquake," in *Proceedings of the Fifteenth International Conference on Soil Mechanics and Geotechnical Engineering*, Istanbul, Turkey, August 2001.

[4] T. Tobita, S. Iai, M. G. Wang et al., "Preliminary report of the Mid Niigata Prefecture, Japan, earthquake in 2004," *Journal of Japan Society for Natural Disaster Science*, vol. 23, no. 4, pp. 595–602, 2005, in Japanese.

[5] Z. Cao, L.-Q. Hou, X. Yuan et al., "Characteristics of liquefaction-induced damages during Wenchuan Ms 8.0 earthquake," *Rock and Soil Mechanics*, vol. 31, no. 11, pp. 3549–3555, 2010, in Chinese.

[6] S. A. Ashford, R. W. Boulanger, J. L. Donahue et al., *Geotechnical Quick Report on the Kanto Plain Region during the March 11, 2011, Off Pacific Coast of Tohoku Earthquake, Japan*, GEER Association Report No. GEER, Geotechnical Extreme Events Reconnaissance (GEER), Tokyo, Japan, 2011.

[7] A. Bobet, "Effect of pore water pressure on tunnel support during static and seismic loading," *Tunnelling and Underground Space Technology*, vol. 18, no. 4, pp. 377–393, 2003.

[8] S. E. Kattis, D. E. Beskos, and A. H. D. Cheng, "2D dynamic response of unlined and lined tunnels in poroelastic soil to harmonic body waves," *Earthquake Engineering & Structural Dynamics*, vol. 32, no. 1, pp. 97–110, 2003.

[9] S. A. S. Youakim, S. E. E. El-Metewally, and W. F. Chen, "Nonlinear analysis of tunnels in clayey/sandy soil with a concrete lining," *Engineering Structures*, vol. 22, no. 2, pp. 707–722, 2000.

[10] A. Amorosi and D. Boldini, "Numerical modeling of the transverse dynamic behavior of circular tunnels in clayey soils," *Soil Dynamics and Earthquake Engineering*, vol. 29, no. 6, pp. 1059–1072, 2009.

[11] S. B. Kojic and M. Trifunac, "Transient pressures in hydrotechnical tunnels during earthquakes," *Earthquake Engineering and Structural Dynamics*, vol. 16, no. 4, pp. 523–539, 1988.

[12] H. Dobashi, E. Ochiai, T. Ichimura et al., "3D FE analysis of seismic response of complicated large-scale ramp tunnel structure," in *Proceedings of the ECCOMAS Thematic Conference on Computational Methods in Structural Dynamics and Earthquake Engineering*, pp. 13–16, Rethymno, Crete, Greece, 2007.

[13] H. Yu, Y. Yuan, and A. Bobet, "Multiscale method for long tunnels subjected to seismic loading," *International Journal for Numerical and Analytical Methods in Geomechanics*, vol. 37, no. 4, pp. 374–398, 2013.

[14] H. Yu, Y. Yuan, Z. Qiao et al., "Seismic analysis of a long tunnel based on multi-scale method," *Engineering Structures*, vol. 49, no. 2, pp. 572–587, 2013.

[15] W. U. Yongxin, Y. Gao, and D. Li, "Simulation of spatially correlated earthquake ground motions for engineering purposes," *Earthquake Engineering and Engineering Vibration*, vol. 10, no. 2, pp. 163–173, 2011.